Macromodeling of Electric Machines from Ab Initio Models

Ajay Pratap Yadav, *Student Member, IEEE,* Tuncay Altun, *Student Member, IEEE,* Ramtin Madani, *Member, IEEE,* and Ali Davoudi, *Senior Member, IEEE*

***Abstract*—We extract the lumped-parameter model of a wound-rotor synchronous machine from its physics-based magnetic-equivalent circuit model. Model extraction is formulated as a weighted least square optimization with nonlinear constraints in which time-domain trajectories of flux linkages, currents, and the electromagnetic torque are used as input data to obtain the parameters of $qd0$ model of the machine. The resulting problem is non-convex and cannot be solved using standard methods. The optimization problem is, therefore, convexified using second-order cone programming relaxation. The solution to the relaxed problem is used as an initial point for the interior-point method, leading to a reliable framework. Accurate estimations on stator resistance, leakage and mutual inductances in stator and rotor, rotor speed, effective turns-ratio between the field and stator windings, and the number of poles are obtained. Estimated parameters are validated against measured and estimated values reported in literature, and are used to develop a behavioral $qd0$ macromodel of the machine.**

***Index Terms*—Convex relaxation, magnetic-equivalent circuit, parameter estimation, second-order cone programming, wound-rotor synchronous machine.**

I. Introduction

Electric machine models can be classified into lumped-parameter models, such as abc phase-domain models, $qd0$ models, or voltage-behind reactance models [1], and those based on the first principles of physics (Maxwell equations), such as finite-element methods (FEM) or magnetic equivalent circuits (MEC). Lumped-parameter macromodels are suitable for system-level studies, drive-controller design, or hardware-in-the-loop applications [1], [2]. FEM models are highly accurate and closely mimic the hardware, but they are computationally expensive and mainly used for the final design verification. MEC modeling is an intuitive approach based on the circuit theory. Herein, we extract a lumped-parameter behavioral $qd0$ model using data generated by the MEC model, thereby breaking the compromise between model fidelity and simulation speed. We use a mesh-based MEC model of a wound-rotor synchronous machine (WRSM) [3]–[6] as it exhibits better numerical properties than its nodal-based counterpart [7]. WRSMs are used in various applications, e.g., aircraft generators, ship propulsion, and wind turbines [8]. $qd0$ model extraction is analogous to replacing the spatially-distributed reluctance network of the MEC model with equivalent lumped-parameter components (see Figure 1).

This work was supported by the National Science Foundation under Grant 1509804. Tuncay Altun was supported, in part, by the National Science Foundation under award ECCS-1809454. Authors are with the Department of Electrical Engineering, University of Texas, Arlington, TX, 76019 USA (e-mail: ajay.yadav@mavs.uta.edu; tuncay.altun@mavs.uta.edu; ramtin.madani@uta.edu; davoudi@uta.edu).

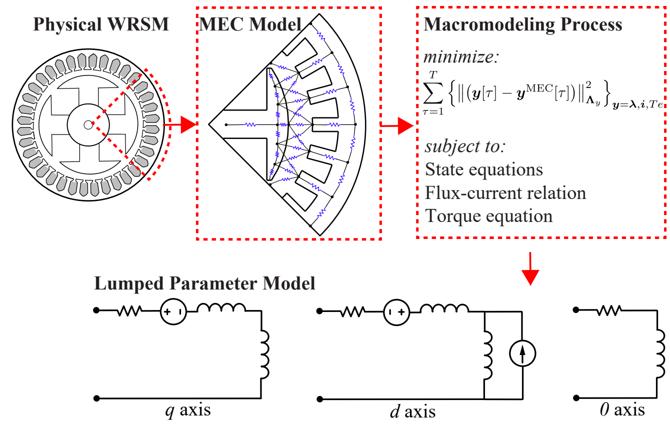

Fig. 1. $qd0$ model extraction from the MEC model of a WRSM.

IEEE Std-115 [9] documents an array of tests to identify synchronous machine parameters. Since it is not always feasible to run all the necessary tests, various techniques estimate machine parameters using transient measurements [10]–[14]. In the absence of hardware measurement, high-fidelity physics-based models, that closely mimic the experimental prototype, can be used instead. Furthermore, detailed models provide access to a host of variables that might not be available experimentally due to a limited sensory. [15] and [16] have used FEM models to determine the parameters of equivalent circuits for an induction machine. [17] has used the data from a pulse test applied to the FEM model of a synchronous machine to obtain its lumped-parameter model. However, MEC models have not yet been exploited for such macromodeling purposes. We formulate the parameter extraction process as a weighted least-square problem with nonlinear constraints such that minimizes the mismatch between trajectories produced by the MEC model and those predicted by the $qd0$ model.

Due to the presence of nonlinear equality constraints the proposed optimization problem is non-convex and cannot be solved reliably using standard interior-point method (IPM) solvers [18]–[20]. To eliminate the need for initialization we propose a hybrid optimization framework based on second-order cone programming (SOCP) relaxation. We relax the original problem and feed the resulting solution to IPM in order arrive to a fully-feasible and globally optimal solution [21]. The contributions of this paper are summarized below:

- We have recovered machine parameters, namely stator

resistance, rotor speed, stator leakage inductance, q-axis magnetizing inductance, d-axis magnetizing inductance, equivalent turns-ratio between the field and the stator windings, and the number of poles. Extracted parameters are compared against those values reported in literature.
- The model extraction is formulated as a non-convex optimization problem using a hybrid SOCP and IPM approach.
- The extracted $qd0$ model is validated against the MEC model, and shown to capture dominant dynamical modes with more than 20 times faster model execution.

The outline of the paper is as follows. Section II is a preliminary review on the symbols and notations used throughout the paper. Section III presents the dynamic MEC model and the target $qd0$ model for WRSM. Section IV elaborates a discrete $qd0$ model for WRSM, and formulates the parameter extraction process as a non-convex optimization problem. Section V presents SOCP relaxation and IPM formulations. Section VI studies the implementation process and results. Finally, Section VII concludes the paper.

II. Notation

Matrices and vectors are presented as bold uppercase and lowercase variables, respectively (e.g., $\mathbf{X}$ or $\mathbf{x}$). $\mathbf{x}_i$ denotes the i^{th} element of vector $\mathbf{x}$. $\mathbf{X}_{ij}$ denotes the element in the i^{th} row and j^{th} column of matrix $\mathbf{X}$. $\mathbb{R}^n$ is the set of column vectors of size $n \times 1$. $\mathbb{R}^{m\times n}$ is the set of matrices of size $m \times n$. $\mathbb{S}^n$ denotes the set of symmetric matrices of size n. $\mathbf{0}_m$ and $\mathbf{1}_m$ represent vectors of size $m \times 1$ with all their elements as 0 and 1, respectively. Similarly, $\mathbf{0}_{m\times n}$ represents a matrix of size $m \times n$ with all its element equal to 0. $\boldsymbol{I}_n$ is an identity matrix of size n. $||\mathbf{x}||_2$ denotes the Euclidean norm of the vector $\mathbf{x}$. $\mathrm{diag}(\mathbf{x})$ gives a diagonal matrix with elements of the vector $\mathbf{x}$ along its diagonal. $\mathbf{diag}(\mathbf{X})$ gives a vector with its elements the same as the diagonal of the input matrix. $\mathbf{diag}(\mathbf{X}, \mathbf{Y})$ produces a block diagonal matrix with input matrices along its diagonal. $(\cdot)^\top$ indicates the transpose operation. $\mathbf{tr}(\mathbf{X})$ denotes the trace of an input matrix $\mathbf{X}$. $||\mathbf{x}||^2_{\mathbf{Z}}$ represents $\mathbf{x}^\top\mathbf{Z}\mathbf{x}$. $\langle \mathbf{X}, \mathbf{Y}\rangle$ stands for the inner product of matrices $\mathbf{X}$ and $\mathbf{Y}$. $^-$ denotes the square of a variable, e.g., $\overline{x}$ represents x^2 for a scalar x and $\overline{\mathbf{x}}$ is a vector with elements of $\mathbf{x}$ squared. $()^{\frac{1}{2}}$ of a vector denotes an element-wise square root operation. $\circ$ and $\otimes$ denotes element-wise product and kronecker product, respectively.

III. Ab Initio and lumped-parameter WRSM models

A. Dynamic MEC Model

This section presents a concise overview of the mesh-based MEC model of the WRSM in [3]–[6]. We have selected the static MEC model in [3] and formed a dynamic MEC model using the procedure laid out in [6]. Therein, the field current and rotor speed are assumed constant. Damper windings are ignored in [3]–[5]. Different segments of stator, rotor, and airgap are modeled using flux tubes to form a magnetic circuit, as seen in Figure 1. Reluctance formulation is based on the geometry and permeability information of respective flux tubes [6]. Kirchhoff's voltage law on individual loops gives

$$\overline{\boldsymbol{\mathcal{R}}}\boldsymbol{\Phi} = \boldsymbol{\mathcal{F}}, \tag{1}$$

where $\overline{\boldsymbol{\mathcal{R}}} \in \mathbb{S}^{nl}$ is the matrix of reluctances, $\boldsymbol{\Phi} \in \mathbb{R}^{nl}$ is vector of flux terms in each loop, $\boldsymbol{\mathcal{F}} \in \mathbb{R}^{nl}$ is the vector of MMF sources, and nl is the number of loops. Note that due to the rotor motion, the reluctances of the flux tubes in the airgap region in matrix $\overline{\boldsymbol{\mathcal{R}}}$ changes with time and should be recalculated at every step. The elements of $\boldsymbol{\mathcal{F}}$ can be obtained as the product of winding turns and currents for each magnetic loop. One can get the flux linkages, $\boldsymbol{\lambda}_{abcs}$, using [5]

$$\boldsymbol{\lambda}_{abcs} = P\mathbf{N}^\top_{abcs}\boldsymbol{\Phi}_{st}, \tag{2}$$

where P is the number of poles, $\mathbf{N}_{abcs}$ is the turns matrix for stator windings, and $\boldsymbol{\Phi}_{st}$ represents the flux in loops corresponding to stator segments.

[6] has reformulated (1) such that flux linkages, $\boldsymbol{\lambda}_{abcs}$, are the inputs and winding currents, $\boldsymbol{i}_{abcs}$, are the output.

$$\begin{bmatrix} \overline{\boldsymbol{\mathcal{R}}} & -c_{scl}\mathbf{N}_{abcs}(\boldsymbol{K_s})^{-1} \\ c_{scl}\boldsymbol{K_s}\mathbf{N}^\top_{abcs} & \mathbf{0} \end{bmatrix} \begin{bmatrix} \boldsymbol{\Phi} \\ \boldsymbol{i}_{qd0s}/c_{scl} \end{bmatrix} = \begin{bmatrix} \mathbf{N}_{fld} & \mathbf{0} \\ \mathbf{0} & c_{scl}\boldsymbol{I}_3/P \end{bmatrix} \begin{bmatrix} i_{fld} \\ \boldsymbol{\lambda}_{qd0s} \end{bmatrix}. \tag{3}$$

The idea is to incorporate the machine dynamics into the otherwise static relation of current and flux in (1). $\boldsymbol{i}_{qd0s}$ and $\boldsymbol{\lambda}_{qd0s}$ are the currents and flux linkages of the stator windings in the rotor reference frame. $\boldsymbol{z}_{qd0} = \boldsymbol{K_s}\boldsymbol{z}_{abc}$, where $\boldsymbol{z}$ represents flux linkages, currents, or voltages, and $\boldsymbol{K_s}$ is the reference frame transformation matrix [1]. $\mathbf{N}_{fld}$ is the turns matrix for the field winding. i_{fld} is the field current. c_{scl} is a scaling factor to condition (3). Equation (3) can be solved to obtain currents, $\boldsymbol{i}_{qd0s}$, for given flux linkages, $\boldsymbol{\lambda}_{qd0s}$.

State-space representation of a synchronous machine in the rotor reference-frame is [1]

$$\frac{d\lambda_{qs}}{dt} = v_{qs} - r_s i_{qs} - \omega_r\lambda_{ds}, \tag{4a}$$

$$\frac{d\lambda_{ds}}{dt} = v_{ds} - r_s i_{ds} + \omega_r\lambda_{qs}, \tag{4b}$$

$$\frac{d\lambda_{0s}}{dt} = v_{0s} - r_s i_{0s}. \tag{4c}$$

v_{qs}, v_{ds}, and v_{0s} are the q-axis, d-axis, and 0-axis voltage terms. r_s is the stator resistance, and ω_r is the rotor speed. Dynamic MEC model solves (3) and (4) in tandem. The electromagnetic torque is calculated using [5]

$$T_e^{\text{MEC}} = \left(\frac{P}{2}\right)^2 \sum_{j=1}^{na}\left(\frac{\phi_{aj}}{P_{aj}}\right)^2 \frac{\partial P_{aj}}{\partial\theta_r}, \tag{5}$$

where ϕ_{aj} and P_{aj} represent flux and permeance for the j^{th} loop in the airgap region. na is the number of airgap loops (changing with the rotor position), and θ_r is the rotor position.

B. $qd0$ Model

State-space representation of a lumped-parameter model is the same as (4). However, the relation between flux linkages and currents is formulated as [1]

$$\lambda_{qs} = (L_{ls}+L_{mq})i_{qs}, \tag{6a}$$

$$\lambda_{ds} = (L_{ls}+L_{md})i_{ds} + \frac{2}{3}\frac{N_{fld}}{N_s}L_{md}i_{fld}, \tag{6b}$$

$$\lambda_{0s} = L_{ls}i_{0s}. \tag{6c}$$

L_{ls} is the leakage inductance of stator, L_{mq} and L_{md} are the q- and d-axis magnetizing inductances, respectively. N_{fld} and N_s are the lumped equivalency of spatially-distributed field winding and stator winding, respectively. The electromagnetic torque becomes

$$T_e = \frac{3P}{4}(\lambda_{ds}i_{qs} - \lambda_{qs}i_{ds}) \ . \tag{7}$$

$qd0$ parameter extraction from the MEC model is analogous to replacing the flux linkage and current relation in (3) with (6).

IV. Setting up the Model Extraction Procedure

In order to extract the $qd0$ model from the MEC model, one can compare trajectories generated from (3), (4), and (5) with those predicted by (6), (4), and (7) and minimize their mismatch. This requires one to discretize the $qd0$ model.

A. Discretizing Machine Dynamics

While a host of methods are available, (e.g., Tustin's [22]), in this work, the forward Euler method is adopted for its simplicity. The discretized state trajectory for a general dynamic system $\frac{d\mathbf{x}}{dt} = f(\mathbf{x})$ using the forward Euler method is

$$\mathbf{x}[\tau+1] = \mathbf{x}[\tau] + \Delta T \times f(\mathbf{x}) \ . \tag{8}$$

$\mathbf{x}$ is the state, ΔT is the sampling time, and τ is the time instance. The $qd0$ model in (4), (6), and (7) is discretized as

$$\boldsymbol{\lambda}[\tau+1] = \boldsymbol{A}\boldsymbol{\lambda}[\tau] + \boldsymbol{R}\boldsymbol{i}[\tau] + \boldsymbol{v}[\tau], \tag{9a}$$

$$\boldsymbol{\lambda}[\tau] = \boldsymbol{L}\boldsymbol{i}[\tau] + \boldsymbol{\ell}\, i_{fld}, \tag{9b}$$

$$Q \times T_e[\tau] = \frac{3}{4}\boldsymbol{\lambda}^\top[\tau]\boldsymbol{M}\boldsymbol{i}[\tau], \tag{9c}$$

where $\boldsymbol{\lambda}[\tau] \in \mathbb{R}^3$ and $\boldsymbol{i}[\tau] \in \mathbb{R}^3$ are the flux linkages and currents, respectively, in rotor reference frame at time instance τ. The $qd0$ subscript is dropped for brevity. $\boldsymbol{v}[\tau]$ in (9a) is the $qd0$ voltage terms times the sampling time, $\boldsymbol{v}[\tau] = \boldsymbol{v}_{qd0}[\tau] \times \Delta T$. Matrices $\boldsymbol{A}$, $\boldsymbol{R}$, $\boldsymbol{L}$, $\boldsymbol{\ell}$, $\boldsymbol{M}$, and Q in (9) are defined as

$$\boldsymbol{A} \triangleq \begin{bmatrix} 1 & -a & 0 \\ a & 1 & 0 \\ 0 & 0 & 1 \end{bmatrix}, \ \boldsymbol{R} \triangleq \begin{bmatrix} -r & 0 & 0 \\ 0 & -r & 0 \\ 0 & 0 & -r \end{bmatrix}, \tag{10a}$$

$$Q \triangleq \frac{1}{P}, \qquad \boldsymbol{L} \triangleq \begin{bmatrix} l_1 & 0 & 0 \\ 0 & l_2 & 0 \\ 0 & 0 & l_3 \end{bmatrix}, \tag{10b}$$

$$\boldsymbol{\ell} \triangleq \begin{bmatrix} 0 \\ l_4 \\ 0 \end{bmatrix}, \quad \boldsymbol{M} \triangleq \begin{bmatrix} 0 & -1 & 0 \\ 1 & 0 & 0 \\ 0 & 0 & 0 \end{bmatrix}, \tag{10c}$$

where $a \triangleq \omega_r\Delta T$, $r \triangleq r_s\Delta T$, $l_1 \triangleq L_{ls}+L_{mq}$, $l_2 \triangleq L_{ls}+L_{md}$, $l_3 \triangleq L_{ls}$, and $l_4 \triangleq \frac{2}{3}\frac{N_{fld}}{N_s}L_{md}$. The model extraction problem presented in following sections aims to determine the parameters $(a, r, l_1, l_2, l_3, l_4, Q)$ based on which, ω_r, r_s, L_{ls}, L_{mq}, L_{md}, $\frac{N_{fld}}{N_s}$, and P can be uniquely determined.

B. Problem Formulation

Supposed that we are given the vectors $\boldsymbol{\lambda}^{\text{MEC}}[\tau]$, $\boldsymbol{i}^{\text{MEC}}[\tau]$, and $T_e^{\text{MEC}}[\tau]$ throughout a discrete time horizon $\tau \in \{1, 2, \ldots \mathsf{T}\}$, representing flux linkages, currents, and torque data from the MEC model, respectively. Then, the parameter extraction for a $qd0$ model from the MEC data can be formulated as the following optimization problem:

$$\textbf{minimize} \ \sum_{\tau=1}^{T} \left\|\boldsymbol{\lambda}[\tau] - \boldsymbol{\lambda}^{\text{MEC}}[\tau]\right\|^2_{\boldsymbol{\Lambda}_\alpha} + \sum_{\tau=1}^{T} \left\|\boldsymbol{i}[\tau] - \boldsymbol{i}^{\text{MEC}}[\tau]\right\|^2_{\boldsymbol{\Lambda}_\beta} + \sum_{\tau=1}^{T} \gamma\left(T_e[\tau] - T_e^{\text{MEC}}[\tau]\right)^2 \tag{11a}$$

subject to

$$\boldsymbol{\lambda}[\tau+1] = \boldsymbol{\lambda}[\tau] + a \times \Big[-\lambda_2[\tau], \lambda_1[\tau], 0\Big]^\top - r \times \boldsymbol{i}[\tau] + \boldsymbol{v}[\tau], \quad \tau = 1, 2, \ldots, \mathsf{T}-1 \tag{11b}$$

$$\boldsymbol{\lambda}[\tau] = \text{diag}\{[l_1, l_2, l_3]\}\boldsymbol{i}[\tau] + l_4 \times i_{fld}, \quad \tau = 1, 2, \ldots, \mathsf{T} \tag{11c}$$

$$Q \times T_e[\tau] = \frac{3}{4}\boldsymbol{\lambda}^\top[\tau]\Big[-i_2[\tau], i_1[\tau], 0\Big]^\top, \ \tau = 1, 2, \ldots, \mathsf{T} \tag{11d}$$

variables

$$\left\{\boldsymbol{\lambda}[\tau] \in \mathbb{R}^3, \boldsymbol{i}[\tau] \in \mathbb{R}^3, T_e[\tau] \in \mathbb{R}\right\}_{\tau=1}^{\tau=T},$$
$$a, l_1, l_2, l_3, l_4, r, Q \in \mathbb{R}.$$

The 3×3 matrices $\boldsymbol{\Lambda_\alpha}$ and $\boldsymbol{\Lambda_\beta}$ are defined as

$$\boldsymbol{\Lambda_\alpha} \triangleq \begin{bmatrix} \alpha_1 & 0 & 0 \\ 0 & \alpha_2 & 0 \\ 0 & 0 & \alpha_3 \end{bmatrix}, \ \boldsymbol{\Lambda_\beta} \triangleq \begin{bmatrix} \beta_1 & 0 & 0 \\ 0 & \beta_2 & 0 \\ 0 & 0 & \beta_3 \end{bmatrix}. \tag{12}$$

where $(\alpha_1, \alpha_2, \alpha_3)$, $(\beta_1, \beta_2, \beta_3)$ and γ are user-defined non-negative weights given to flux, current and torque data, respectively.

The objective function (11a) represents the total mismatch between the MEC and $qd0$ trajectories. The equality constraint in (11b) represents the state equation for the $qd0$ model. Constraints in (11c) and (11d) form the flux linkage-current relationship and torque expressions, respectively. The auxiliary variable $Q = 1/P$ is defined to reduce the order of torque equation from three (cubic) to two (quadratic), which will help in the following SOCP formulation. To summarize, the optimization problem in (11) minimizes the sum of scaled residuals for trajectories of flux linkages, currents, and torque to uniquely obtain $\boldsymbol{\lambda}$, $\boldsymbol{i}$, T_e, $\boldsymbol{A}$, $\boldsymbol{R}$, $\boldsymbol{L}$, $\boldsymbol{\ell}$, and Q subject to the constraints in (11a) - (11d).

V. Convex Relaxation and Numerical Search

Without proper initialization, local search algorithms may fail to converge to a globally optimal solution or even a feasible point. To address this issue, we use SOCP relaxation followed by IPM to reliably solve the problem (11a) - (11d). The proposed convex relaxation is explained next.

A. SOCP Relaxation

The original optimization problem in (11) is non-convex due to the presence of bilinear terms:

- $a\ \lambda_2[\tau]$, $a\ \lambda_1[\tau]$ and $r\ \boldsymbol{i}[\tau]$ in (11b);
- $l_1\ i_1[\tau]$, $l_2\ i_2[\tau]$ and $l_3\ i_3[\tau]$ in (11c); as well as
- $\lambda_1[\tau]\ i_2[\tau]$, $\lambda_2[\tau]\ i_1[\tau]$ and $Q\ T_e[\tau]$ in (11d).

The aforementioned nonlinearity can be tackled by introducing new variable (i.e., lifting the problem). To this end, define:

$$\boldsymbol{f}[\tau] \triangleq \Big[a\lambda_2[\tau],\ -a\lambda_1[\tau],\ 0\Big]^\top, \tag{13a}$$
$$\boldsymbol{h}[\tau] \triangleq r \times \boldsymbol{i}[\tau], \tag{13b}$$
$$\boldsymbol{z}[\tau] \triangleq \mathrm{diag}\{[l_1,\ l_2,\ l_3]\}\ \boldsymbol{i}[\tau], \tag{13c}$$
$$\boldsymbol{w}[\tau] \triangleq \Big[\lambda_1[\tau]i_2[\tau], \lambda_2[\tau]i_1[\tau],\ 0\Big]^\top, \tag{13d}$$
$$\theta[\tau] \triangleq Q \times T_e[\tau] \tag{13e}$$

The aforementioned auxiliary terms participate in (11b) - (11d) and can be used to simplify them as we will demonstrate later. However, in order to streamline the relaxation process it is necessary to reformulate the definitions in (13) as follows:

$$\begin{aligned}&\sqrt{(\bar{a}-a^2)\left(\bar{\lambda}_2[\tau]-\lambda_2[\tau]^2\right)} = |f_1[\tau]-a\lambda_2[\tau]|,\\ &\sqrt{(\bar{a}-a^2)\left(\bar{\lambda}_1[\tau]-\lambda_1[\tau]^2\right)} = |f_2[\tau]-a\lambda_1[\tau]|,\\ &f_3[\tau]=0 \qquad \tau=1,2,\ldots,\mathsf{T}\end{aligned} \tag{14a}$$

$$\begin{aligned}&\sqrt{\left(\bar{\lambda}_1[\tau]-\lambda_1[\tau]^2\right)\left(\bar{i}_2[\tau]-i_2[\tau]^2\right)} = |w_1[\tau]-\lambda_1[\tau]i_2[\tau]|,\\ &\sqrt{\left(\bar{\lambda}_2[\tau]-\lambda_2[\tau]^2\right)\left(\bar{i}_1[\tau]-i_1[\tau]^2\right)} = |w_2[\tau]-\lambda_2[\tau]i_1[\tau]|,\\ &w_3[\tau]=0 \qquad \tau=1,2,\ldots,\mathsf{T}\end{aligned} \tag{14b}$$

$$\begin{aligned}&\sqrt{\mathrm{diag}\{[\bar{l}_1-l_1^2,\ \bar{l}_2-l_2^2,\ \bar{l}_3-l_3^2]\}(\bar{\boldsymbol{i}}[\tau]-\mathrm{diag}\{\boldsymbol{i}[\tau]\}\boldsymbol{i}[\tau])}\\ &\qquad = |\boldsymbol{z}[\tau]-\mathrm{diag}\{[l_1,\ l_2,\ l_3]\}\ \boldsymbol{i}[\tau]| \quad \tau=1,2,\ldots,\mathsf{T}\end{aligned} \tag{14c}$$

$$\begin{aligned}&\sqrt{(\bar{r}-r^2)(\bar{\boldsymbol{i}}[\tau]-\mathrm{diag}\{\boldsymbol{i}[\tau]\}\boldsymbol{i}[\tau])}\\ &\qquad = |\boldsymbol{h}[\tau]-r\times\boldsymbol{i}[\tau]| \quad \tau=1,2,\ldots,\mathsf{T}\end{aligned} \tag{14d}$$

$$\begin{aligned}&\sqrt{(\bar{Q}-Q^2)(\bar{T}_e[\tau]-T_e[\tau]^2)}\\ &\qquad = |\theta[\tau]-Q\times\bar{T}_e[\tau]| \quad \tau=1,2,\ldots,\mathsf{T}\end{aligned} \tag{14e}$$

where

$$\bar{l}_1 \triangleq l_1^2,\quad \bar{l}_2 \triangleq l_3^2,\quad \bar{l}_3 \triangleq l_3^2, \tag{15a}$$
$$\bar{a} \triangleq a^2,\quad \bar{r} \triangleq r^2,\quad \bar{Q} \triangleq Q^2, \tag{15b}$$
$$\bar{\boldsymbol{\lambda}}[\tau] \triangleq \mathrm{diag}\{\boldsymbol{\lambda}[\tau]\}\boldsymbol{\lambda}[\tau], \qquad \tau=1,2,\ldots,\mathsf{T} \tag{15c}$$
$$\bar{\boldsymbol{i}}[\tau] \triangleq \mathrm{diag}\{\boldsymbol{i}[\tau]\}\boldsymbol{i}[\tau], \qquad \tau=1,2,\ldots,\mathsf{T} \tag{15d}$$
$$\bar{T}_e[\tau] \triangleq T_e[\tau]^2 \qquad \tau=1,2,\ldots,\mathsf{T} \tag{15e}$$

It can be easily observed that the equations in (14) are equivalent to (13). In what follows, we will transform all of equalities in (14) and (15), in order to arrive to a convex relaxation:

$$\begin{aligned}\textbf{minimize}\ &\sum_{\tau=1}^{T}\boldsymbol{\alpha}^\top\left(\bar{\boldsymbol{\lambda}}[\tau]+\mathrm{diag}\{\boldsymbol{\lambda}^{\mathrm{MEC}}[\tau]\}(\boldsymbol{\lambda}^{\mathrm{MEC}}[\tau]-2\boldsymbol{\lambda}[\tau])\right)\\ &+\sum_{\tau=1}^{T}\boldsymbol{\beta}^\top\left(\bar{\boldsymbol{i}}[\tau]+\mathrm{diag}\{\boldsymbol{i}^{\mathrm{MEC}}[\tau]\}(\boldsymbol{i}^{\mathrm{MEC}}[\tau]-2\boldsymbol{i}[\tau])\right)\\ &+\sum_{\tau=1}^{T}\gamma\left(\bar{T}_e[\tau]-2\ T_e^{\mathrm{MEC}}[\tau]T_e[\tau]+T_e^{\mathrm{MEC}}[\tau]^2\right)\end{aligned} \tag{16a}$$

subject to

$$\boldsymbol{\lambda}[\tau+1]=\boldsymbol{\lambda}[\tau]-\boldsymbol{f}[\tau]-\boldsymbol{h}[\tau]+\boldsymbol{v}[\tau], \quad \tau=1,2,\ldots,\mathsf{T}-1 \tag{16b}$$
$$\boldsymbol{\lambda}[\tau]=\boldsymbol{z}[\tau]+l_4\times i_{fld}, \quad \tau=1,2,\ldots,\mathsf{T} \tag{16c}$$
$$\theta[\tau]=\frac{3}{4}(w_2[\tau]-w_1[\tau]), \quad \tau=1,2,\ldots,\mathsf{T} \tag{16d}$$

$$\bar{l}_1 \ge l_1^2,\quad \bar{l}_2 \ge l_3^2,\quad \bar{l}_3 \ge l_3^2, \tag{16e}$$
$$\bar{a} \ge a^2,\quad \bar{r} \ge r^2,\quad \bar{Q} \ge Q^2, \tag{16f}$$
$$\bar{\boldsymbol{\lambda}}[\tau] \ge \mathrm{diag}\{\boldsymbol{\lambda}[\tau]\}\boldsymbol{\lambda}[\tau], \quad \tau=1,2,\ldots,\mathsf{T} \tag{16g}$$
$$\bar{\boldsymbol{i}}[\tau] \ge \mathrm{diag}\{\boldsymbol{i}[\tau]\}\boldsymbol{i}[\tau], \quad \tau=1,2,\ldots,\mathsf{T} \tag{16h}$$
$$\bar{T}_e[\tau] \ge T_e[\tau]^2 \quad \tau=1,2,\ldots,\mathsf{T} \tag{16i}$$

$$\begin{aligned}&\sqrt{(\bar{a}-a^2)\left(\bar{\lambda}_2[\tau]-\lambda_2[\tau]^2\right)} \ge |f_1[\tau]-a\lambda_2[\tau]|,\\ &\sqrt{(\bar{a}-a^2)\left(\bar{\lambda}_1[\tau]-\lambda_1[\tau]^2\right)} \ge |f_2[\tau]-a\lambda_1[\tau]|,\\ &f_3[\tau]=0 \qquad \tau=1,2,\ldots,\mathsf{T}\end{aligned} \tag{16j}$$

$$\begin{aligned}&\sqrt{\left(\bar{\lambda}_1[\tau]-\lambda_1[\tau]^2\right)\left(\bar{i}_2[\tau]-i_2[\tau]^2\right)} \ge |w_1[\tau]-\lambda_1[\tau]i_2[\tau]|,\\ &\sqrt{\left(\bar{\lambda}_2[\tau]-\lambda_2[\tau]^2\right)\left(\bar{i}_1[\tau]-i_1[\tau]^2\right)} \ge |w_2[\tau]-\lambda_2[\tau]i_1[\tau]|,\\ &w_3[\tau]=0 \qquad \tau=1,2,\ldots,\mathsf{T}\end{aligned} \tag{16k}$$

$$\begin{aligned}&\sqrt{\mathrm{diag}\{[\bar{l}_1-l_1^2,\ \bar{l}_2-l_2^2,\ \bar{l}_3-l_3^2]\}(\bar{\boldsymbol{i}}[\tau]-\mathrm{diag}\{\boldsymbol{i}[\tau]\}\boldsymbol{i}[\tau])}\\ &\qquad \ge |\boldsymbol{z}[\tau]-\mathrm{diag}\{[l_1,\ l_2,\ l_3]\}\ \boldsymbol{i}[\tau]| \quad \tau=1,2,\ldots,\mathsf{T}\end{aligned} \tag{16l}$$

$$\begin{aligned}&\sqrt{(\bar{r}-r^2)(\bar{\boldsymbol{i}}[\tau]-\mathrm{diag}\{\boldsymbol{i}[\tau]\}\boldsymbol{i}[\tau])}\\ &\qquad \ge |\boldsymbol{h}[\tau]-r\times\boldsymbol{i}[\tau]| \quad \tau=1,2,\ldots,\mathsf{T}\end{aligned} \tag{16m}$$

$$\begin{aligned}&\sqrt{(\bar{Q}-Q^2)(\bar{T}_e[\tau]-T_e[\tau]^2)}\\ &\qquad \ge |\theta[\tau]-Q\times\bar{T}_e[\tau]| \quad \tau=1,2,\ldots,\mathsf{T}\end{aligned} \tag{16n}$$

variables

$$\left\{\boldsymbol{\lambda}[\tau],\boldsymbol{i}[\tau],\bar{\boldsymbol{\lambda}}[\tau],\bar{\boldsymbol{i}}[\tau],\boldsymbol{f}[\tau],\boldsymbol{h}[\tau],\boldsymbol{z}[\tau],\boldsymbol{w}[\tau]\in\mathbb{R}^3\right\}_{\tau=1}^{T},$$
$$\left\{T_e[\tau],\bar{T}_e[\tau]\in\mathbb{R}\right\}_{\tau=1}^{T},$$
$$a,l_1,l_2,l_3,l_4,r,Q,\bar{a},\bar{l}_1,\bar{l}_2,\bar{l}_3,\bar{l}_4,\bar{r},\bar{Q}\in\mathbb{R}.$$

Equality constraints in (16b) - (16d) are the same as those in (11b) - (11d) which describe the WRSM model equations. The inequalities in (16e) - (16k) implicitly impose (13) - (15) to preserve equivalency to the original problem in (11) and the convexified problem in (16). It is straightforward to observe that (16e) - (16k) are convex if formulated as linear matrix inequalities:

$$\begin{bmatrix} \bar{a} & f_k[\tau] \\ f_k[\tau] & \bar{\lambda}_{3-k}[\tau] \end{bmatrix} \succeq \begin{bmatrix} (-1)^{3-k} a \\ \lambda_{3-k}[\tau] \end{bmatrix} \begin{bmatrix} (-1)^{3-k} a \\ \lambda_{3-k}[\tau] \end{bmatrix}^\top k=1,2 \quad (17a)$$

$$\begin{bmatrix} \bar{\lambda}_k[\tau] & w_k[\tau] \\ w_k[\tau] & \bar{i}_{3-k}[\tau] \end{bmatrix} \succeq \begin{bmatrix} \lambda_k[\tau] \\ i_{3-k}[\tau] \end{bmatrix} \begin{bmatrix} \lambda_k[\tau] \\ i_{3-k}[\tau] \end{bmatrix}^\top \quad k=1,2 \quad (17b)$$

$$\begin{bmatrix} \bar{l}_k & z_k[\tau] \\ z_k[\tau] & \bar{i}_k[\tau] \end{bmatrix} \succeq \begin{bmatrix} l_k \\ i_k[\tau] \end{bmatrix} \begin{bmatrix} l_k \\ i_k[\tau] \end{bmatrix}^\top \quad k=1,2,3 \quad (17c)$$

$$\begin{bmatrix} \bar{r} & h_k[\tau] \\ h_k[\tau] & \bar{i}_k[\tau] \end{bmatrix} \succeq \begin{bmatrix} r \\ i_k[\tau] \end{bmatrix} \begin{bmatrix} r \\ i_k[\tau] \end{bmatrix}^\top \quad k=1,2,3 \quad (17d)$$

$$\begin{bmatrix} \bar{Q} & \theta[\tau] \\ \theta[\tau] & \bar{T}_{e,k}[\tau] \end{bmatrix} \succeq \begin{bmatrix} Q \\ T_{e,k}[\tau] \end{bmatrix} \begin{bmatrix} Q \\ T_{e,k}[\tau] \end{bmatrix}^\top \quad k=1,2,3 \quad (17e)$$

The optimization problem in (16) is a relaxation and its solution may not be feasible for the original problem in (11). Nonetheless, the SOCP solution can be used as an initial point for any general purpose IPM solvers.

As an alternative to IPM, [23] proposes a penalization method for finding feasible and near-optimal solutions to problems of the form (11). This approach is regarded as penalized convex relaxation. Let $\hat{\boldsymbol{x}} = \left(\{\hat{\boldsymbol{\lambda}}[\tau], \hat{\boldsymbol{i}}[\tau], \hat{T}_e[\tau]\}_{\tau=1}^{\mathsf{T}}, \hat{a}, \hat{l}_1, \hat{l}_2, \hat{l}_3, \hat{r}, \hat{Q}\right)$ be an optimal solution for the SOCP relaxation problem (16). If $\hat{\boldsymbol{x}}$ is not feasible for the original nonconvex problem, one can incorporate a penalty term of the form

$$\begin{aligned} &\kappa\left(\{\hat{\boldsymbol{\lambda}}[\tau], \hat{\boldsymbol{i}}[\tau], \hat{T}_e[\tau]\}_{\tau=1}^{\mathsf{T}}, \hat{a}, \hat{l}_1, \hat{l}_2, \hat{l}_3, \hat{r}, \hat{Q}\right) \\ &= \eta_a(\bar{a} - 2\hat{a}a + \hat{a}^2) + \eta_r(\bar{r} - 2\hat{r}r + \hat{r}^2) \\ &+ \eta_Q(\bar{Q} - 2\hat{Q}Q + \hat{Q}^2) + \eta_{l_1}(\bar{l}_1 - 2\hat{l}_1 l_1 + \hat{l}_1^2) \\ &+ \eta_{l_2}(\bar{l}_2 - 2\hat{l}_2 l_2 + \hat{l}_2^2) + \eta_{l_3}(\bar{l}_3 - 2\hat{l}_3 l_3 + \hat{l}_3^2) \\ &+ \eta_\lambda \sum_{\tau=1}^{T} (\mathbf{1}_3^\top \bar{\boldsymbol{\lambda}}[\tau] - 2\hat{\boldsymbol{\lambda}}^\top[\tau]\boldsymbol{\lambda}[\tau] + \hat{\boldsymbol{\lambda}}^\top[\tau]\hat{\boldsymbol{\lambda}}[\tau]) \\ &+ \eta_i \sum_{\tau=1}^{T} (\mathbf{1}_3^\top \bar{\boldsymbol{i}}[\tau] - 2\hat{\boldsymbol{i}}^\top[\tau]\boldsymbol{i}[\tau] + \hat{\boldsymbol{i}}^\top[\tau]\hat{\boldsymbol{i}}[\tau]) \\ &+ \eta_{T_e} \sum_{\tau=1}^{T} (\bar{T}_e[\tau] - 2\hat{T}_e[\tau]T_e[\tau] + \hat{T}_e^2). \end{aligned} \quad (18)$$

in the objective function of relaxation and solve additional rounds of SOCP to obtain fully feasible points with satisfactory objective values. In (18), the parameters $\eta_a, \eta_r, \eta_Q, \eta_{l_1}, \eta_{l_2}, \eta_{l_3}, \eta_\lambda, \eta_i, \eta_{T_e} \geq 0$ are user-defined.

VI. Model Generation and Verification

A. System Setup

The MEC model of a 2 kW WRSM is adopted from [3]. The machine is constructed using M19 steel laminations, and copper conductors are used for stator and field windings. The optimization experiments are run on a workstation equipped with Intel(R) Core i7-6700 CPU (4 cores) at 3.40 GHz and 32 GB of RAM with Windows 10. The SOCP optimization problem in (16) is solved using the SDPT3 4.0 [25] and MOSEK [26] solver running on CVX [27] in the MATLAB 2017b environment. Local search is implemented using MATPOWER Interior Point Solver (MIPS) [28].

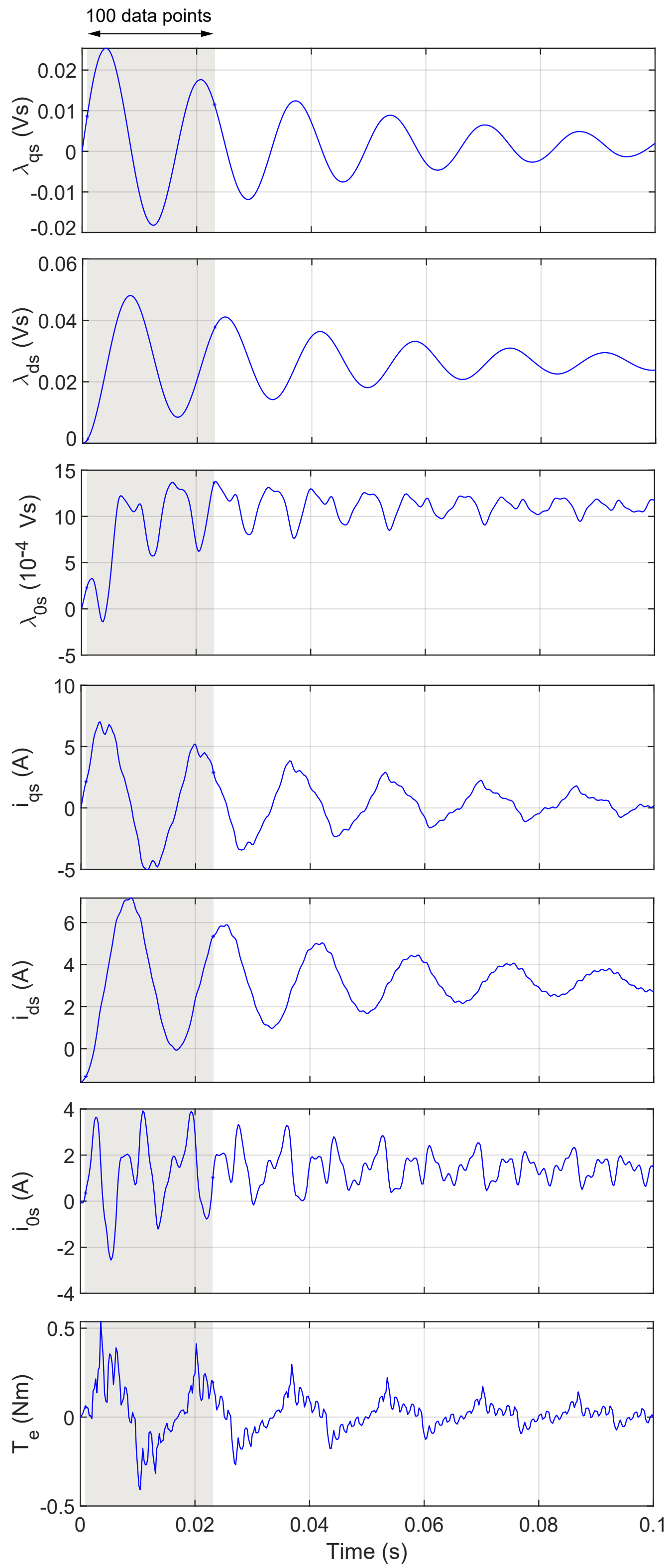

Fig. 2. Time-domain transients for flux linkages, currents, and electromagnetic torque. Operating condition is $i_{fld} = 0.25$ A, $\omega_r = 3600$ RPM, $v_{qs} = 10$ V, $v_{ds} = 0$ V, and $v_{0s} = 0.25$ V. The sampling length is $\Delta T = 2.22 \times 10^{-4}$s. Only the highlighted sections of the data are used for model extraction.

TABLE I
MACHINE PARAMETERS EXTRACTED USING IPM

Parameter	MEC [3], [24]	Hardware [3]	Estimated Parameters	%Mismatch (wrt MEC)	%Mismatch (wrt Hardware)
ω_r*(rad/sec)	376.99	376.99	377.10	0.02	0.02
$r_s(\Omega)$	0.1729**	0.21	0.1738	0.52	17.23
L_{ls} (mH)	0.83	0.90	0.75	9.06	16.13
L_{mq} (mH)	3.06	3.07	2.94	3.74	4.05
L_{md} (mH)	4.71	4.46	4.74	0.66	6.30
$\frac{N_{fld}}{N_s}$	10.94	Not available	11.16	2.00	-
P	4	4	3.90***	-	-

*Electrical angular speed of the rotor. **Directly obtained from the MEC model. ***P, takes even integer values.

TABLE II
SOCP RESULTS

Parameter	MEC [3], [24]	Estimated Parameters	%Mismatch (w.r.t. MEC model)
ω_r*(rad/sec)	376.99	376.98	0.0005
$r_s(\Omega)$	0.1729**	0.1729	0
L_{ls} (mH)	0.83	0.27	67.47
L_{mq} (mH)	3.06	3.38	10.45
L_{md} (mH)	4.71	5.19	10.19
$\frac{N_{fld}}{N_s}$	10.94	10.23	6.50
P	4	4.44***	-

*Electrical angular speed of the rotor. **Directly obtained from the MEC model. ***The number of poles, P, takes even integers.

B. Training Data Generated by the Dynamic MEC Model

We have considered an unbalanced operation of the WRSM to generate training data with non-zero zero-sequence flux linkage and current components. Zero initial conditions are assumed for the states. Figure 2 shows the flux linkages, currents, and electromagnetic torque waveforms generated using the MEC model. The highlighted portions of plots in Figure 2, that include 100 data points, are used in parameter extraction. More data points will improve the solution, albeit at the expense of computational time.

C. Model Extraction Procedure

The optimization problem in Section V-A is first solved using SOCP. The result is used as an initial condition for IPM. The tuning gains for SOCP are $\Lambda_{\boldsymbol{\alpha}} = \Lambda_{\boldsymbol{\beta}} = \mathbf{diag}\,\{1, 1, 0.001\}$ and $\gamma = 1$. A flat initial condition is assumed with all unknown variables set to 1. The length of the time horizon is $T = 100$. SOCP solves (16) over a convexified version of the feasible set of (11). Table II shows the SOCP results. The obtained set is not necessarily a feasible point (e.g., see L_{ls}), but can be a good initial point for IPM. In comparison, in all of our experiments, five rounds of penalized relaxation resulted in feasible points and parameters similar to those of IPM.

The tuning gains for IPM are $\Lambda_{\boldsymbol{\alpha}} = \mathbf{diag}\left\{10^4, 10^4, 10^4\right\}$, $\Lambda_{\boldsymbol{\beta}} = \mathbf{diag}\,\{0.001, 0.001, 0.001\}$, and $\gamma = 0.1$. Table I tabulates the parameters extracted by IPM after solving (11). These parameters are compared against those reported in [3] (corresponding to MEC-BH1 model). Reference value of the stator resistance, $r_s = 0.1729\ \Omega$, is directly obtained in the MEC model [3] using equivalent length and area of the windings. The reference value for the effective turns ratio between the field and stator windings, $\frac{N_{fld}}{N_s}$, is taken from that reported in [24]. As seen in Table I, the percentage mismatch for the estimated parameters w.r.t. MEC reference values is highest for L_{ls} at 9.96%, whereas the rest of the parameters are estimated within 3.8% accuracy. Estimation error with respect to the hardware values is obviously higher given the inherent mismatch between the original MEC model and the hardware prototype in [3]. It should be noted that parameters reported for MEC model should be considered for comparative purpose.

In the problem formulation in (11) and (16), transients of flux linkages, currents, and electromagnetic torque are also considered as optimization variables. The IPM solution recovers these variables along with the machine parameters. Figure 3 compares the time-domain transients of input MEC data and the trajectories obtained by the IPM in the optimization process. As expected, the optimization algorithm aims to minimize the mismatch between the trajectories of the input MEC model and the extracted $qd0$ model.

D. MEC vs $qd0$ Model Comparison

The MEC model of the WRSM had been validated against a hardware prototype [3]. Herein, we reproduce Figure 10a of [3] to compare our $qd0$ model against the validated MEC model. The WRSM is run under an open circuit with $i_{fld} = 1$ A and $\omega_r = 1000$ RPM. Figure 4 shows the phase-a voltage waveform for the extracted $qd0$ model, and that obtained by the static MEC model. The harmonic effects of the spatial distribution of stator slots are evident in the MEC model. The voltage waveform produced by both models are in agreement.

Next, the $qd0$ model and the dynamic MEC model are simulated with $i_{fld} = 1$ A, $\omega_r = 3600$ RPM, and a balanced load R_{load} = 20 Ω. The phase-a transients, as seen in Figure 5, show that the resulting $qd0$ model mimic the essential dynamics of the MEC model. The physical time for a 5-cycle (83.3 ms) simulation run for the MEC and $qd0$ models are 0.8362 s and 0.0377 s, respectively. The $qd0$ model is more than 20 times faster than the dynamic MEC model.

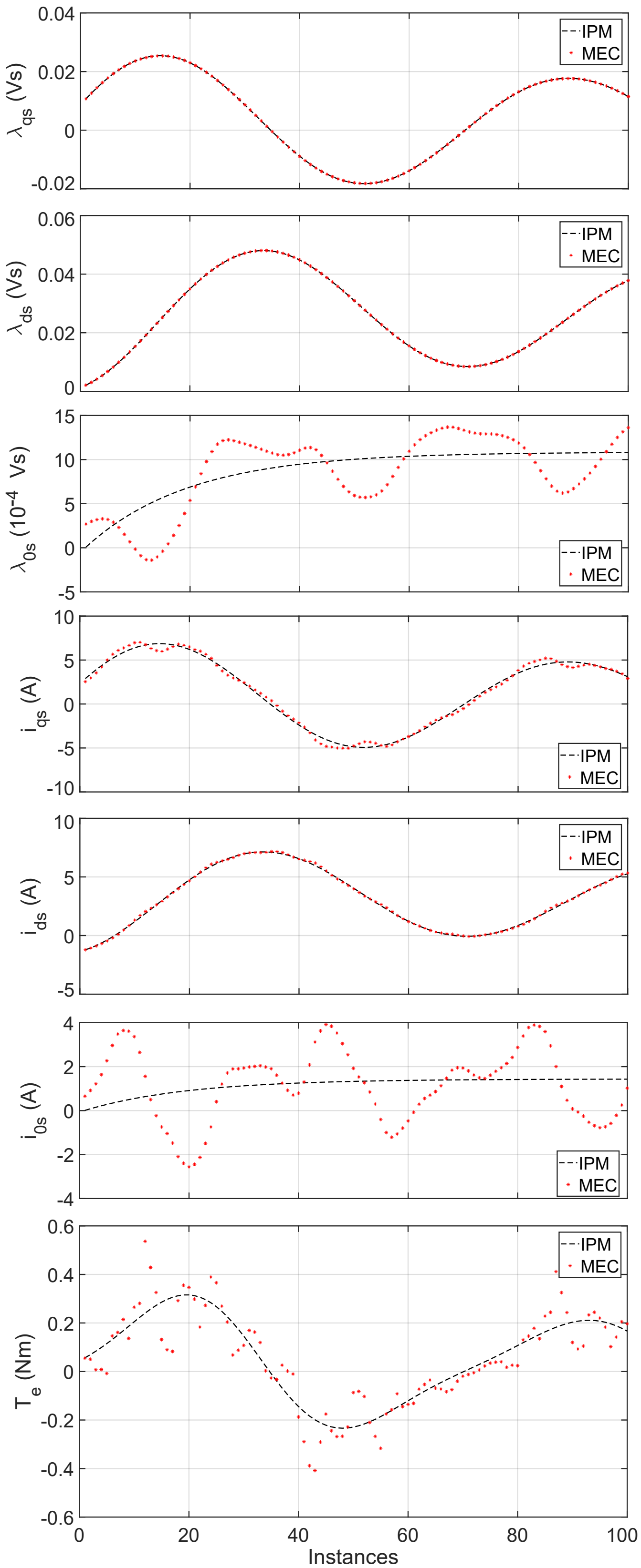

Fig. 3. Trajectories obtained from IPM compared with the input MEC data.

VII. Summary

The macromodel of a 2 kW WRSM is successfully extracted from its dynamic MEC model. The parameter extraction process is formulated as an optimization problem; This problem is first covexified using the SOCP relaxation method and, then, the resulting solution is used to initialize the IPM solver. We have successfully extracted all the machine parameters within 4% accuracy with respect to the original MEC model; The leakage inductance, L_{ls}, was estimated within 10% accuracy. The extracted $qd0$ model is compared against MEC model, and exhibits very high fidelity despite an appreciable gain in the simulation speed. Future work will study the effect of magnetic saturation in the macromodel extraction.

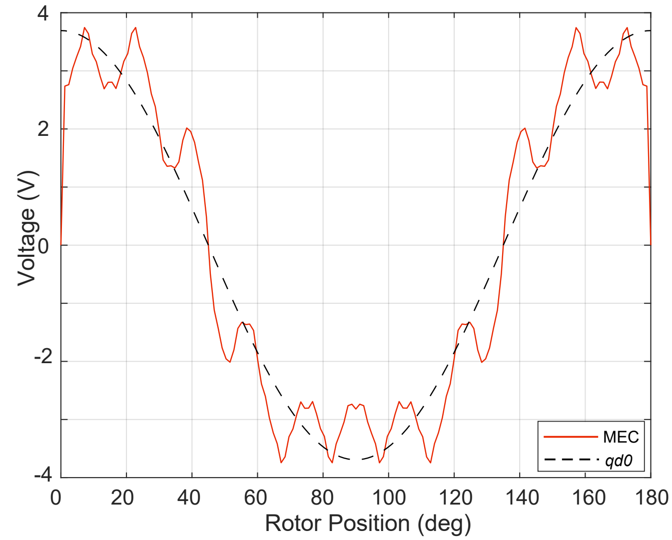

Fig. 4. Open-circuit operation of the static MEC model in [3] and the resulting $qd0$ model (i_{fld} = 1 A, $\omega_r = 1000$ RPM).

VIII. Acknowledgment

We wish to thank the researchers at Purdue University for making their codes available online. We wish to thank Nuh Erdogan, from University College Cork, for fruitful comments.

References

[1] P. Krause, O. Wasynczuk, S. D. Sudhoff, and S. Pekarek, *Analysis of electric machinery and drive systems*. John Wiley & Sons, 2013.

[2] N. Roshandel Tavana and V. Dinavahi, "A general framework for fpga-based real-time emulation of electrical machines for hil applications," *IEEE Transactions on Industrial Electronics*, vol. 62, no. 4, pp. 2041–2053, April 2015.

[3] M. L. Bash and S. Pekarek, "Analysis and validation of a population-based design of a wound-rotor synchronous machine," *IEEE Transactions on Energy Conversion*, vol. 27, no. 3, pp. 603–614, Sep. 2012.

[4] M. L. Bash, J. M. Williams, and S. D. Pekarek, "Incorporating motion in mesh-based magnetic equivalent circuits," *IEEE Transactions on Energy Conversion*, vol. 25, no. 2, pp. 329–338, June 2010.

[5] M. L. Bash and S. D. Pekarek, "Modeling of salient-pole wound-rotor synchronous machines for population-based design," *IEEE Transactions on Energy Conversion*, vol. 26, no. 2, pp. 381–392, June 2011.

[6] R. Wang, S. Pekarek, M. L. Bash, A. Larson, and R. V. Maaren, "Incorporating dynamics in a mesh-based magnetic equivalent circuit model of synchronous machines," *IEEE Transactions on Energy Conversion*, vol. 30, no. 3, pp. 821–832, Sep. 2015.

[7] H. W. Derbas, J. M. Williams, A. C. Koenig, and S. D. Pekarek, "A comparison of nodal-and mesh-based magnetic equivalent circuit models," *IEEE Transactions on Energy Conversion*, vol. 24, no. 2, pp. 388–396, May 2009.

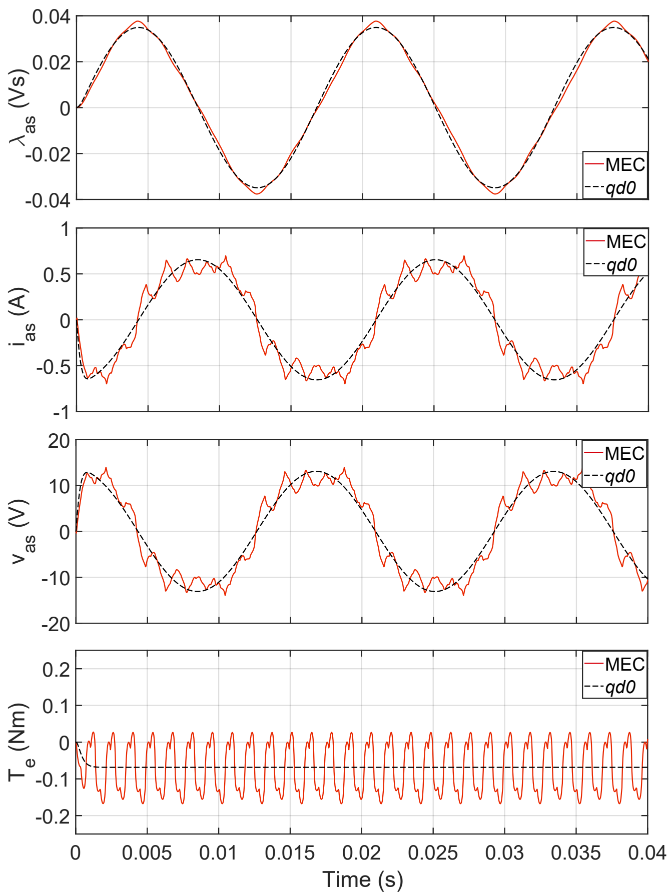

Fig. 5. Flux linkage, current, voltage, and electric torque for the extracted $qd0$ model compared against the MEC model, when connected to a balanced resistive load (i_{fld} = 1 A, ω_r = 3600 RPM, R_{load} = 20 Ω).

[8] G. Friedrich and A. Girardin, "Integrated starter generator," *IEEE Industry Applications Magazine*, vol. 15, no. 4, pp. 26–34, July 2009.

[9] "Ieee guide for test procedures for synchronous machines part iacceptance and performance testing part ii-test procedures and parameter determination for dynamic analysis," *IEEE Std 115-2009*, 2010.

[10] M. Karrari and O. P. Malik, "Identification of physical parameters of a synchronous generator from online measurements," *IEEE Transactions on Energy Conversion*, vol. 19, no. 2, pp. 407–415, June 2004.

[11] E. Kyriakides, G. T. Heydt, and V. Vittal, "Online parameter estimation of round rotor synchronous generators including magnetic saturation," *IEEE Transactions on Energy Conversion*, vol. 20, no. 3, pp. 529–537, Sep. 2005.

[12] J. J. Sanchez-Gasca, C. J. Bridenbaugh, C. E. J. Bowler, and J. S. Edmonds, "Trajectory sensitivity based identification of synchronous generator and excitation system parameters," *IEEE Transactions on Power Systems*, vol. 3, no. 4, pp. 1814–1822, Nov 1988.

[13] G. Valverde, E. Kyriakides, G. T. Heydt, and V. Terzija, "Nonlinear estimation of synchronous machine parameters using operating data," *IEEE Transactions on Energy Conversion*, vol. 26, no. 3, pp. 831–839, Sep. 2011.

[14] T. Boileau, N. Leboeuf, B. Nahid-Mobarakeh, and F. Meibody-Tabar, "Online identification of pmsm parameters: Parameter identifiability and estimator comparative study," *IEEE Transactions on Industry Applications*, vol. 47, no. 4, pp. 1944–1957, July 2011.

[15] Ping Zhou, J. Gilmore, Z. Badics, and Z. J. Cendes, "Finite element analysis of induction motors based on computing detailed equivalent circuit parameters," *IEEE Transactions on Magnetics*, vol. 34, no. 5, pp. 3499–3502, Sep. 1998.

[16] A. Repo, P. Rasilo, A. Niemenmaa, and A. Arkkio, "Identification of electromagnetic torque model for induction machines with numerical magnetic field solution," *IEEE Transactions on Magnetics*, vol. 44, no. 6, pp. 1586–1589, June 2008.

[17] O. Makela, A. Repo, and A. Arkkio, "Parameter estimation for synchronous machines using numerical pulse test within finite element analysis," in *18th International Conference on Electrical Machines*, 2008, pp. 1–5.

[18] V. H. Quintana, G. L. Torres, and J. Medina-Palomo, "Interior-point methods and their applications to power systems: a classification of publications and software codes," *IEEE Transactions on Power Systems*, vol. 15, no. 1, pp. 170–176, Feb 2000.

[19] P. Beyhaghi, D. Cavaglieri, and T. Bewley, "Delaunay-based derivative-free optimization via global surrogates, part i: linear constraints," *Journal of Global Optimization*, vol. 66, no. 3, pp. 331–382, 2016.

[20] M. Kojima, S. Mizuno, and A. Yoshise, *A Primal-Dual Interior Point Algorithm for Linear Programming*. New York, NY: Springer New York, 1989, pp. 29–47. [Online]. Available: https://doi.org/10.1007/978-1-4613-9617-8_2

[21] Y. Weng, Q. Li, R. Negi, and M. Ilic, "Semidefinite programming for power system state estimation," in *IEEE Power and Energy Society General Meeting*, 2012, pp. 1–8.

[22] C. A. Rojas, J. I. Yuz, M. Aguirre, and J. Rodriguez, "A comparison of discrete-time models for model predictive control of induction motor drives," in *IEEE International Conference on Industrial Technology (ICIT)*, 2015, pp. 568–573.

[23] R. Madani, M. Kheirandishfard, J. Lavaei, and A. Atamtürk, "Penalized conic relaxations for quadratically constrained quadratic programming," *Preprint*, Jun. 2019. [Online]. Available: http://www.uta.edu/faculty/madanir/penalty_paper.pdf

[24] R. Wang, S. Pekarek, and M. Bash, "Alternative excitation strategies for a wound rotor synchronous machine drive," in *IEEE Energy Conversion Congress and Exposition (ECCE)*, 2012, pp. 2300–2307.

[25] R. H. Tütüncü, K. C. Toh, and M. J. Todd, "Solving semidefinite-quadratic-linear programs using sdpt3," *Mathematical Programming*, vol. 95, no. 2, pp. 189–217, Feb 2003. [Online]. Available: https://doi.org/10.1007/s10107-002-0347-5

[26] MOSEK-Aps, *The MOSEK optimization toolbox for MATLAB manual. Version 8.1.*, 2017. [Online]. Available: http://docs.mosek.com/8.1/toolbox/index.html

[27] M. Grant and S. Boyd, "CVX: Matlab software for disciplined convex programming, version 2.1," http://cvxr.com/cvx, Mar. 2014.

[28] R. D. Zimmerman and H. Wang, "Matpower interior point solver mips 1.3 user's manual," 2016.